Journal of Catalysis 281 (2011) 88–97

Contents lists available at ScienceDirect

Journal of Catalysis

journal homepage: www.elsevier.com/locate/jcat

Synthesis, characterisation and catalytic performance of nanocrystalline Co_3O_4 for gas-phase chlorinated VOC abatement

Beatriz de Rivas, Rubén López-Fonseca, Cristina Jiménez-González, José I. Gutiérrez-Ortiz *

Department of Chemical Engineering, Faculty of Science and Technology, Universidad del País Vasco/EHU, P.O. Box 644, E-48080 Bilbao, Spain

ARTICLE INFO

Article history:
Received 10 February 2011
Revised 4 April 2011
Accepted 5 April 2011
Available online 10 May 2011

Keywords:
VOC oxidation
1,2-Dichlorethane
Ethylene dichloride
Co_3O_4
Synthesis
Crystallite size

ABSTRACT

Several nanocrystalline Co_3O_4 catalysts were investigated for their activity and selectivity during the oxidation of 1,2-dichloroethane, which was selected as a model chlorinated volatile organic compound. A wide number of synthesis routes starting from cobalt(II) nitrate were examined, namely calcination of the precursor salt, solid-state reaction, precipitation and sol–gel. The catalysts prepared by precipitation decomposed the chlorinated feed at the lowest temperatures. Activity was observed to be chiefly governed by a small crystallite size which may give rise to more easily accessible active sites (oxygen $-O^-$ or $O^{2-}-$ species), which were not present on the more highly crystalline Co_3O_4 catalysts. Additionally, surface Lewis acidity played a relevant catalytic role. Interestingly, the behaviour of some of the nanocrystalline oxides was superior to that of supported noble metal catalysts and other bulk oxide catalysts. Conversion to deep oxidation products was complete (CO_2, HCl and Cl_2), and no appreciable deactivation with time on stream was noticed.

1. Introduction

Over the past several years, environmental legislation has imposed increasingly stringent limits on permitted atmospheric emission levels. In particular, the release of volatile organic compounds (VOCs) has received much attention. VOCs are a widely ranging class of chemicals commonly occurring in many commercial waste streams and containing over 300 compounds. Their release has widespread environmental implications and has been linked to the increase in photochemical smog, the depletion in atmospheric ozone and the production of ground-level ozone. Additionally, many VOCs have highly noxious effects on human health. The emission sources associated with industrial activity (manufacture of organic chemicals and polymers, vent air from operations in which VOCs are used for cleaning and degreasing purposes in metal processing, machining and finishing, and exhaust air from ground water and/or soil remediation processes) reveal a wide variety of compounds with different chemical compositions, though the ease or difficulty involved in removing them varies considerably. In this sense, chlorinated VOCs, which have enjoyed widespread acceptance as reagents and solvents due to their compatibility with most substrate materials and non-flammability, are, on account of their high stability, amongst the most difficult to abate compounds by catalytic combustion.

An alternative to commonly applied but expensive noble metals is transition metal oxides. Despite their high activity for the abatement of chlorinated VOCs, the disadvantages associated with noble metals (high cost, low thermal stability and susceptibility to poisoning [1]) cannot be overcome. Thus, substantial efforts are currently being made to develop transition metal oxides catalysts with a comparable activity. Cobalt oxide catalysts are effective low-temperature combustion catalysts of non-chlorinated hydrocarbons [2–5], carbon monoxide [6,7] and diesel soot [8]. However, much less consideration has been given to investigating the applicability of this class of catalysts for the gas-phase oxidation of chlorinated VOCs [9,10].

The active behaviour of Co-based catalysts in the above applications, typically as Co_3O_4, is most likely related to high bulk oxygen mobility and the facile formation of highly active oxygen (O^- or O^{2-}) species. These properties are mainly related to crystallite size. Hence, the controlled preparation of Co_3O_4 nanoparticles (1–50 nm) has attracted considerable interest owing to its impact on governing their ultimate performance and applications. In the present work, the suitability of cobalt oxide catalysts for the abatement of chlorinated VOCs was investigated. Particularly, the catalytic behaviour of nanocrystalline Co_3O_4 systems on the total oxidation of 1,2-dichloroethane, which was chosen as a model chlorinated VOC, was examined in a fixed-bed flow reactor. 1,2-Dichloroethane ($C_2H_4Cl_2$, DCE), also known in the industry as ethylene dichloride (EDC), is probably one of the most important chlorinated VOCs emitted in gaseous industrial waste streams since it is used as an intermediate for the production of polyvinyl

* Corresponding author. Fax: +34 94 6015963.
E-mail address: joseignacio.gutierrez@ehu.es (J.I. Gutiérrez-Ortiz).

0021-9517/$ - see front matter © 2011 Elsevier Inc. All rights reserved.
doi:10.1016/j.jcat.2011.04.005

chloride, the most produced plastic in the world after polyethylene. Less important uses are as a solvent in textile cleaning and metal degreasing and paint remover, a starting material for paint, varnish, and finish removers, a cleaner for upholstery and carpets, a fumigant, a lead scavenger in antiknock gasoline and as a dispersant for plastics and elastomers such as synthetic rubber.

2. Experimental

2.1. Catalyst preparation

A number of routes including thermal decomposition, solid-state reaction, wet-chemical and sol–gel methods were employed to synthesise bulk cobalt oxide catalysts. Firstly, Co_3O_4 was prepared by simple calcination in air of the selected cobalt precursor (hexahydrated cobalt(II) nitrate, Sigma–Aldrich). This catalyst was denoted as DC. Secondly, the cobalt oxide was prepared by solid-state reaction following two different procedures. Hence, on one hand, the GB catalyst was prepared by grinding a mixture of cobalt(II) nitrate (9 g) with ammonium hydrogen carbonate (Fluka) (6.1 g) with a molar ratio of 2:5 in an agate mortar for 30 min [11]. The solids were washed thoroughly with distilled water and collected by filtration. The GC catalyst was obtained by grinding a mixture of citric acid (5.3 g) (Sigma–Aldrich) with the Co(II) basic carbonate precursor (8.7 g) (Sigma–Aldrich) [12]. The mixture was first premixed by hand grinding for 5 min. The grinding was then carried out in a planetary ball mill (Retsch) at a speed of 600 rpm for 6 h. The as-ground citrate precursors were collected and washed thoroughly.

Co_3O_4 catalysts were also prepared by wet-chemical methods. The first route (OW) consisted of a precipitation–oxidation reaction in an aqueous solution. The precipitation process was conducted by the drop-by-drop addition of 100 ml of a 3.2 M solution of NaOH (Sigma–Aldrich) into an aqueous solution (50 cm^3) of 0.6 M $Co(NO_3)_2{\cdot}6H_2O$ at 50 °C. Next, 100 ml of H_2O_2 (Sigma–Aldrich, 50 wt.%) was also introduced drop-by-drop under constant stirring [13]. The precipitate was then filtered and washed with deionised water. The alternative procedure (CC) involved an aqueous hydroxycarbonate precipitation [12]. Thus, a 1.2 M aqueous (200 cm^3) solution of Na_2CO_3 (Fluka) was added into a 0.5 M aqueous (100 cm^3) solution of cobalt(II) nitrate under vigorous stirring. The temperature was kept at 80 °C during the precipitation (0.5 h), the pH was fixed at 8.5 and the precipitates were collected and washed thoroughly. Finally, a sol–gel method (SG) was employed. The oxide was prepared by an aqueous sol–gel citrate procedure involving complexation of cobalt(II) nitrate (0.1 M, 250 cm^3) and citric acid. An excess of citric acid (3.5 g) was used to ensure complete complexation. Water was removed on a rotary evaporator at 40 °C until the formation of a gel or viscous material. The temperature was then increased up to 70 °C and maintained overnight. A spongy, highly hygroscopic, amorphous citrate was obtained [14].

All the catalyst precursors were dried at 110 °C overnight and then calcined at 300 or 500 °C in static air for 4 h at a heating rate of 1 °C min^{-1}. For the samples calcined at 500 °C, an intermediate calcination at 300 °C for 0.5 h was performed. Next, catalyst pellets with a 0.3–0.5 mm diameter were prepared by a process of compressing the oxide powders into flakes in a hydraulic press (Specac), crushing and sieving. All samples obtained prior to catalytic activity and selectivity experiments were characterised using several analytical techniques.

2.2. Characterisation techniques

Textural properties were evaluated from the nitrogen adsorption–desorption isotherms, determined at −196 °C with a Micromeritics ASAP 2010 apparatus. The specific areas of the samples were determined in line with standard BET procedure, using nitrogen adsorption taken in the relative equilibrium pressure interval of 0.03–0.3. Mean pore size was calculated using the BJH method. The samples were previously degassed overnight under high vacuum conditions. X-ray diffraction (XRD) studies were conducted on a X'PERT-MPD X-ray diffractometer with Cu Kα radiation (λ = 1.5406 Å) and Ni filter. The X-ray tube was operated at 30 kV and 20 mA. Samples were scanned between 20° (2θ) and 70° (2θ), and the X-ray diffraction line positions were determined with a step size of 0.02° and a counting time of 2.5 s per step. Phase identification was conducted by comparison with JCPDS (Joint Committee on Powder Diffraction Standards) database cards. The thermo-oxidative degradation of the cobalt precursors was investigated by means of dynamic thermogravimetry using Setaram Setsys Evolution apparatus under atmospheric pressure. The mass loss and the sample temperature were continuously recorded by a computerised data acquisition system. The studies were carried out from 25 to 550 °C at a constant heating rate of 10 °C min^{-1}. The oxidant stream was dry air (50 cm^3 min^{-1}) flowing downwards onto the cylindrical sample holder.

Raman spectra, acquired using a Leica 50× N Plan (0.75 aperture) lens, were recorded with a Renishaw InVia Raman spectrometer coupled to a Leica DMLM microscope. The spectrometer was equipped with a 514-nm laser (ion-argon laser, Modu-Laser) with a nominal power at the source of 50 mW, with maximum power at the sample of 20 mW. Ten seconds were employed for each spectrum, and 20 scans were accumulated with 10% of the maximum power in the spectral window from 150 to 1150 cm^{-1}.

Temperature-programmed desorption (TPD) of ammonia was performed on a Micromeritics AutoChem 2920 instrument equipped with a quartz U-tube coupled to a thermal conductivity detector. Prior to adsorption experiments, the samples were first pre-treated in a 5%O_2/He stream at 500 °C and then cooled to 100 °C in a He flow (20 cm^3 min^{-1}). Later, the NH_3 adsorption step was performed by admitting a flow of 10%NH_3/He at 100 °C up to saturation. Subsequently, the samples were exposed to a flow of helium (50 cm^3 min^{-1}) for 1 h at 100 °C to remove reversibly and physically bound ammonia from the surface. Finally, desorption was carried out from 100 to 500 °C at a heating rate of 10 °C min^{-1} in an He stream (50 cm^3 min^{-1}). This temperature was maintained for 1 h until the adsorbate was completely desorbed. The amount of gases desorbed was determined by time integration of the TPD curves. Diffuse reflectance (DRIFT) spectra of pyridine adsorbed on the oxide samples were obtained with a Nicolet Protegé 460 ESP spectrometer, equipped with a Spectra-Tech high-temperature chamber and a nitrogen-cooled MCT detector. All spectra were recorded in the range 1700–1300 cm^{-1} averaging 400 scans with a 1 cm^{-1} resolution and analysed using OMNIC software. After the sample was evacuated at 550 °C under high vacuum conditions for 1 h, pyridine was admitted at 200 °C at the equilibrium pressure of 3 mbar. After removing physisorbed pyridine, the spectra were then recorded. Difference spectra were obtained by subtracting the spectrum of the clean sample from the spectra obtained after pyridine adsorption.

Redox behaviour was examined by temperature-programmed reduction (TPR), and the experiments were also conducted on a Micromeritics AutoChem 2920 instrument as well. Firstly, all the samples were pre-treated in an oxygen stream (5%O_2/He) at 500 °C for 1 h and then cooled to room temperature. The reducing gas used in all experiments was 5%H_2/Ar, with a flow rate of 50 cm^3 min^{-1}. The temperature range explored was from room temperature to 500 °C, with a heating rate of 10 °C min^{-1}. This temperature was maintained for 0.5 h. The water produced by reduction was trapped in a cold trap, and consumption of H_2 was quantitatively measured by time integration of the TPR profiles.

During this test, the reduction of Co_3O_4 to Co was assumed to be complete since no hydrogen consumption was registered when a second TPR run was performed. Oxygen storage complete capacity (OSCC) measurements were taken using Micromeritics ASAP 2010 equipment. The samples were first calcined at 500 °C for 1 h in a 5%O_2/He stream to clean the surface and then subjected to a reduction treatment with a pure hydrogen stream at constant temperature (150–350 °C) for 1 h. The sample was then purged with helium, and the measurement of oxygen consumption at 500 °C was taken.

The quantification of chlorine content present in the used catalysts was evaluated by energy disperse X-ray (EDX also known as EDS, or EDAX) analysis using a JEOL JSM-6400 scanning electron microscope coupled with analysis software INCA Energy 350 from Oxford Instruments.

2.3. Catalyst activity determination

Catalytic tests were performed in a bench-scale fixed-bed reactor (Microactivity modular laboratory system provided by PID Eng&Tech S.L.) operated at atmospheric pressure and fully monitored by computer. The reactor was made of quartz with an internal diameter of 10 mm and a height of 300 mm, in which the temperature was controlled with a thermocouple place in the catalyst bed. Typically 0.85 g of catalyst in powdered form (0.3–0.5 mm) was loaded. The catalyst bed was diluted with inert quartz (0.85 g, 1–1.25 mm). The reaction feed consisted of 1000 ppm of DCE in dry air with a total gas flow of 500 cm^3 min^{-1}. The amount and granulometric fraction of catalyst and the total gaseous stream were chosen selected to be in a true kinetic regime, i.e. beyond the internal and external diffusion limits, and to reach a gas hourly space velocity of 15,000 h^{-1}, which corresponds to the conditions usually met in the exhaust gases from industrial units. Catalytic activity was measured over the range 150–500 °C, and conversion data were calculated by the difference between inlet and outlet concentrations. Conversion measurements and product profiles were taken at steady state, typically after 30 min on stream. Product selectivity was calculated based on either chlorine or carbon atoms present in that product divided by the total chlorine or carbon atoms present in the product stream (expressed as %). Feed and effluent streams were analysed using an online 7980A Agilent Technologies gas chromatograph equipped with thermal conductivity (CO and CO_2) and an electron capture detector (chlorinated hydrocarbons). Analysis of HCl and Cl_2 was conducted using ion selective electrode and titration, respectively. Further details on analytical procedures are described elsewhere [15].

3. Results

3.1. Physicochemical characterisation of the Co_3O_4 samples

Thermogravimetric analysis was conducted in order to determine the temperature for the oxidative decomposition of the various cobalt catalytic precursors. As a result, the activation procedure could be defined so as to obtain the desired cobalt oxide (Co_3O_4). Several weight losses were recorded from 110 to 300 °C (not shown here), though no further change in weight was observed at higher temperatures. Thus, calcination at a temperature of at least 300 °C was required to obtain cobalt oxide phases as Co_3O_4. Two calcination temperatures were selected, namely 300 and 500 °C in air for 4 h, to analyse the thermal stability of the oxides. Hence, the samples were denoted as −300, for example DC-300, and as −500, for example DC-500.

The structural properties were characterised by XRD using the JCPDS files as a reference. Fig. 1 shows the XRD patterns of the cobalt samples calcined at 300 and 500 °C. As for the samples activated at the lower temperature, it was checked that all the reflection peaks located at 2θ 31.3°, 36.8°, 44.8°, 59.3° and 65.2° could be perfectly indexed to a pure cubic phase of Co_3O_4 spinel (JCPDS 78-1970), irrespectively of the synthesis route. No diffraction peaks related to a CoO phase were detected [12,16]. The average crystallite size, estimated from the full width half maximum of the characteristic diffraction peaks by applying the Scherrer equation (Table 1), was about 5–6 nm for all the samples except

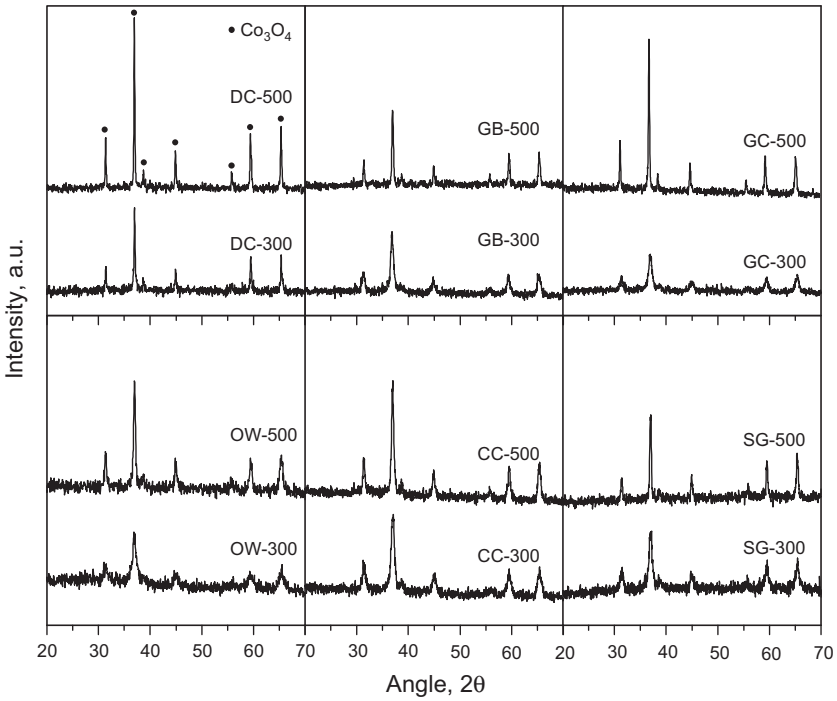

Fig. 1. XRD diffraction patterns of the Co_3O_4 samples.

for DC-300 (18 nm). After calcination at 500 °C, all the samples maintained their structure, i.e. Co_3O_4 cobalt oxide in the absence of other cobalt species. However, significantly more intense well-resolved reflections were noticeable in larger particle sizes (higher crystallinity) [13,17]. The influence of calcination on the crystallite size growth varied depending on the preparation procedure. Hence, the samples obtained by precipitation (CC-500 and OW-500 samples) exhibited a less pronounced growth of crystallite size (Table 1), increasing by a factor of 1.8–2 in comparison with the GC-500 sample whose crystallite size was six times greater. On the other hand, the DC-500 sample showed the largest size with a value of 38 nm.

The evolution of the textural properties as a function of the calcination temperature in terms of specific surface area, pore volume and average pore size is shown in Table 1. As for the samples calcined at 300 °C, the surface area varied between 21 and 80 $m^2\,g^{-1}$. The GC-300 and CC-300 samples had the highest surface area, whereas the DC-300 sample showed the lowest value. Thermal treatment at 500 °C in air provoked notable modifications, involving a progressive drop in the surface area (by 45–85%) and pore volume along with a significant increment in the pore size in some cases. In line with XRD analysis, these results suggested that the samples underwent noticeable sintering. The DC-550 sample was shown to be the most affected catalyst, with a surface area as low as 3 $m^2\,g^{-1}$. In contrast, both CC-500 and OW-500 displayed better behaviour in terms of thermal stability. All the adsorption/desorption isotherms were typical for mesoporous materials, with significantly reduced hysteresis loops for the oxides activated at 500 °C.

Acid properties were evaluated by means of NH_3-TPD analysis, with the corresponding profiles shown in Fig. 2. The total amount of desorbed ammonia, expressed as mmol of adsorbed NH_3 per gram of catalyst and estimated by integrating the area of the TPD curve, was taken as a measurement of the total acid sites concentration. The NH_3-TPD profiles revealed the presence of acid sites with varying strength on each sample. Characteristically, two desorption peaks were observed at 190–200 and 300–305 °C. A shoulder at 250 °C was also evident. However, two additional peaks at 150 and 500 °C were noticed for the OW-500 and CC-500 samples. Hence, the sum of the areas under the first two peaks (150 and 190 °C) was assumed to be the number of weak acid sites, and the sum of the areas under the other two peaks (300 and 500 °C) was associated with the number of strong acid sites. The results are listed in Table 1.

It was observed that the amount of acid sites varied as a function of the preparation method. Hence, the GB-300 sample exhibited the highest total acidity whilst the DC-300 oxide showed a considerably reduced acidity. The area under the TPD curves dropped significantly for all the oxides after calcination at 500 °C (Table 1), thereby showing an overall loss of the total number of acid sites (15–65%). This feature was aligned with surface sintering. The sample CC-500 was the oxide that preserved a larger amount of acid sites (0.34 mmol $NH_3\,g^{-1}$) due to a less noticeable decrease in its surface area. The DC-500 oxide presented the most dramatic decrease in the amount of acid sites in line with the observed severe sintering. As far as acid strength was concerned, it could be concluded that the majority of synthesised oxides exhibited equal amounts of weak and strong acid sites. In contrast, the samples obtained by precipitation (CC and OW) exhibited an appreciably larger amount of strong acid sites, and their distribution was not appreciably modified by the activation temperature. It is important to highlight that to the best of our knowledge, this is the first time that results on surface acidity of bulk Co_3O_4 catalysts have been reported in the technical literature. The nature (Brønsted/Lewis) of the acid sites was investigated by DRIFT spectroscopy of adsorbed pyridine at 200 °C. Infrared spectra were characterised by an intense absorption band at about 1445–1460 cm^{-1} associated with the presence of Lewis sites.

The redox properties of cobalt catalysts were investigated by temperature-programmed reduction with hydrogen. Fig. 3 compares the reduction behaviour of the oxides calcined at 500 °C as a function of the preparation method. Hydrogen consumption profiles were quite similar in most cases, corresponding to a two-step reduction process initiated at approximately 200 °C. The first peak was centred at about 250 °C and was associated with the reduction of Co^{3+} ions to Co^{2+} with the concomitantly structural change to CoO (Eq. (1)), whilst the second peak was located at around 350 °C and attributed to subsequent reduction of CoO to metallic cobalt (Eq. (2)) [18]. Only for the sample DC-500 was the distinction between the two peaks not as evident as in the case of the other cobalt oxides.

$$Co_3O_4 + H_2 \rightarrow 3CoO + H_2O \quad (1)$$

$$3CoO + 3H_2 \rightarrow 3Co + 3H_2O \quad (2)$$

A quantitative evaluation of the amounts of hydrogen consumed during reduction (about 170 μmol $H_2\,g^{-1}$) revealed that in all cases, Co_3O_4 was reduced almost completely into metallic cobalt at about 400 °C (425 °C for DC-500 sample) As predicted by Eqs. (1) and (2), the ratio between the areas of the two peaks was about 1:3. To gain a better understanding of the reducibility of the samples, an attempt was made to quantify the amount of hydrogen consumed in each step. The area under each curve made it possible to estimate the relative fraction of reduced cobalt species with temperature. It was observed that the H_2 consumed at low temperatures (200–300 °C) by CC-500 and OW-500 samples was 25% and 23% of the total amount (peak H_2 uptake at 260–270 °C), respectively, compared with 10–20% for the other samples (peak H_2 uptake at 280–340 °C).

Table 1
Textural, structural and acid properties of the synthesised Co_3O_4 samples.

Catalyst	BET surface area ($m^2\,g^{-1}$)	Pore volume ($cm^3\,g^{-1}$)	Average pore size (Å)	Crystallite size (nm)	Total acidity (mmol $NH_3\,g^{-1}$)	Relative amount of strong sites (%)
DC-300	21	0.06	175	18	0.10	46
DC-500	3	0.004	106	38	0.03	39
GB-300	80	0.30	160	6	0.53	51
GB-500	35	0.07	144	16	0.28	49
GC-300	78	0.24	96	5	0.27	47
GC-500	18	0.05	314	30	0.19	43
OW-300	53	0.13	131	5	0.23	80
OW-500	26	0.05	113	10	0.16	79
CC-300	78	0.25	159	5	0.39	86
CC-500	42	0.13	197	9	0.34	85
SG-300	65	0.16	93	5	0.28	47
SG-500	20	0.04	113	13	0.18	52

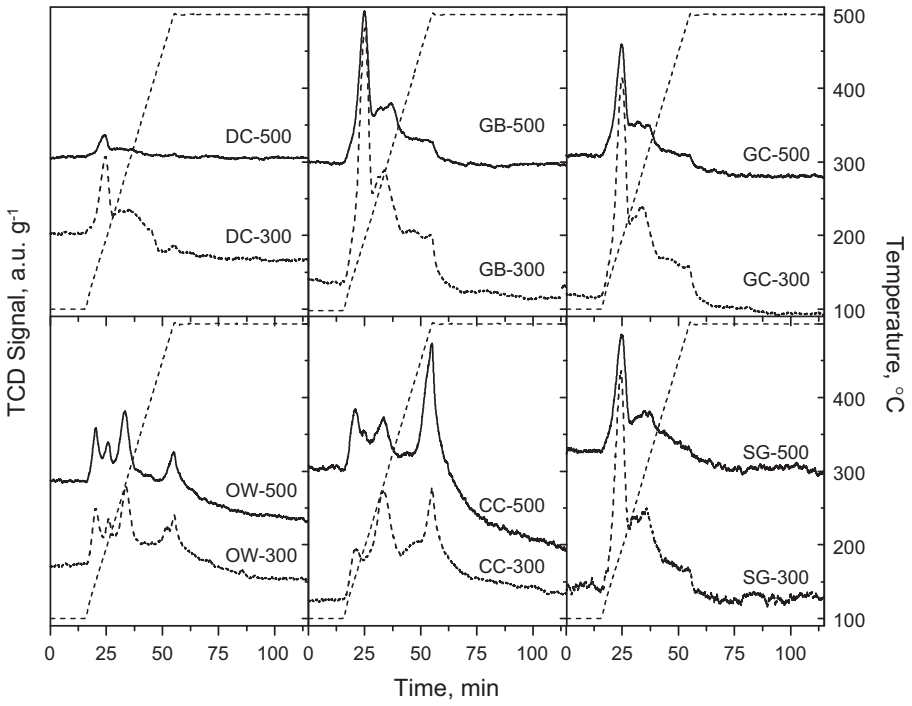

Fig. 2. NH_3-TPD profiles of the Co_3O_4 samples.

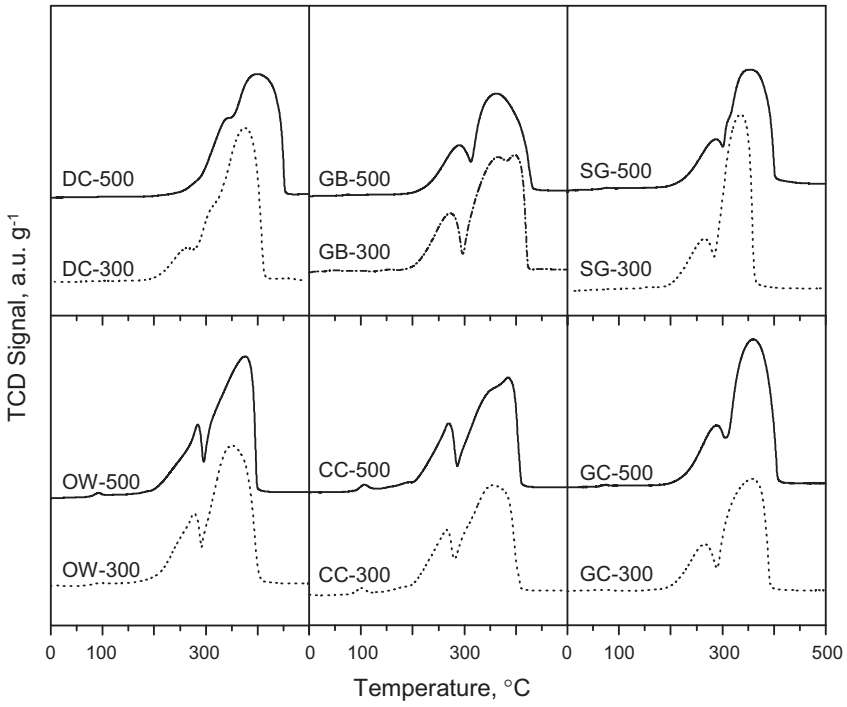

Fig. 3. H_2-TPR profiles of the Co_3O_4 samples.

Furthermore, the reduction of Co_3O_4 in these two samples started at noticeably lower temperatures, with a new small peak at about 100 °C, which was not detected for the other cobalt oxides. This peak was attributed to very active species on the surface formed during the preoxidation treatment [19]. Therefore, it could be concluded that the synthesis of cobalt oxides having a small crystallite size favoured the formation of easily reducible sites, which are less abundant on more highly crystalline Co_3O_4 catalysts.

For the sake of comparison, TPR profiles of the samples calcined at 300 °C are also included in Fig. 3. All of them showed a two-step reduction profile. As expected, it was observed that reducibility was promoted by about 25 °C due to the lower crystallite size of this series of oxides. Interestingly, no differences in reduction temperatures were observed between CC-300 and CC-500 samples, and OW-300 and OW-500 samples. These results were seen to be aligned to less marked growth of the crystallite size, thus revealing

that both precipitation routes led to relatively stable bulk oxides without a noticeable inhibition of reduction after calcination at 500 °C.

3.2. Catalytic performance of Co_3O_4 samples

The oxidation of 1,2-dichloroethane was chosen as a measure to assess the performance of the prepared Co_3O_4 catalysts. 1,2-Dichloroethane was taken as a model for the category of double carbon chlorinated VOCs with a H/Cl ratio of >1. This compound is typically ranked intermediate-high on its ease of destruction when compared, for instance, with double carbon olefins such as dichloroethylene and trichloroethylene [20]. Before testing the activity and selectivity of the cobalt oxide catalysts, the transport effects were evaluated to ensure that experimental results were not significantly influenced by interphase transportation. Calculation of the theoretical external transfer rate of reactants to the catalytic particles (at a typical temperature 300 °C) based on estimated mass-transfer coefficients gave a value three orders of magnitude larger than the measured reaction rates, indicating process conditions were far from external diffusional limitations. The effects of external mass-transfer resistances were experimentally evaluated by repeating a set of process conditions whilst employing a different linear velocity. Results of these experiments indicated that conversion was not affected for linear velocity higher than 7 cm s^{-1}, to within the experimental error. Likewise, estimates of interphase temperature gradients showed fluid–solid differences of less than 1 °C, thereby limiting heat transfer limitation concerns. The possibility of internal pore diffusion was examined by measuring conversions at fixed conditions for catalyst particles of different size. Results showed that pore diffusional resistance was absent for particles less than 1 mm in diameter. Intraparticle mass-transfer resistances were theoretically evaluated by computing effectiveness factors, which were calculated to be greater than 0.98, indicating that intraparticle mass-transfer resistances were not significant. Finally, internal thermal gradients also proved to be negligible over the range of conditions evaluated in this study.

The activity of the bulk catalysts was examined by means of the corresponding ignition or light-off curves between 150 and 500 °C, characterised by the T_{50} and T_{90} parameters (temperature needed to attain 50 and 90% conversion, respectively). The light-off curves are plotted in Fig. 4, whilst the T_{50} and T_{90} values are listed in Table 2. The samples calcined at 500 °C were first examined, since it was *a priori* expected that the oxidation process under the tested experimental conditions would require relatively high reaction temperatures due to the known stability of chlorinated VOCs. The results from the homogeneous reaction (the catalyst was replaced by inert quartz particles) are also included for comparative purposes. DCE conversion in the absence of any catalyst did not start prior to 350 °C and reached only 20% conversion at 500 °C. In contrast, the use of Co_3O_4 oxide as catalyst significantly accelerated the desired reaction, and in all cases the chlorinated compound was completely abated between 325 and 500 °C, which compared very favourably with temperatures in excess of 500 °C, which would be required for thermal combustion.

Table 2
T_{50} and T_{90} values of DCE oxidation over Co_3O_4 samples.

Catalyst	T_{50} (°C)	T_{90} (°C)
DC-500	380	435
GB-500	305	370
GC-500	320	375
OW-500	275	320
CC-500	250	300
SG-500	305	350
No catalyst	>500	≫500

Nevertheless, substantial differences were clearly evident depending on the used synthesis route, thus revealing that the preparation method to be a key factor for obtaining a highly active Co_3O_4 catalyst. Hence, the range at which the 50% conversion was achieved varied between 250 and 380 °C, whereas the temperature for complete removal (90% conversion) was in the 325–500 °C range. The best behaviour was exhibited by the CC-500 sample, which was obtained via aqueous hydroxycarbonate precipitation, with a T_{50} value of 250 °C, whilst the poorest performance was that of the DC-500 oxide showed (T_{50} value of 380 °C). The catalytic activity followed this trend: CC-500 > OW-500 > SG-500 ≈ GB-500 > GC-500 > DC-500. In addition to the CC-500 oxide, the OW-500 sample also emerged as an oxide with an attractive behaviour for DCE oxidation with a T_{50} value of 275 °C. The precipitation routes (via sodium carbonate or sodium hydroxide in the presence of oxygenated water) therefore appeared as adequate methods for preparing active nanocrystalline cobalt oxides for chlorinated VOC abatement. The notable activity of these cobalt oxides indicated that excessively high temperatures were not required.

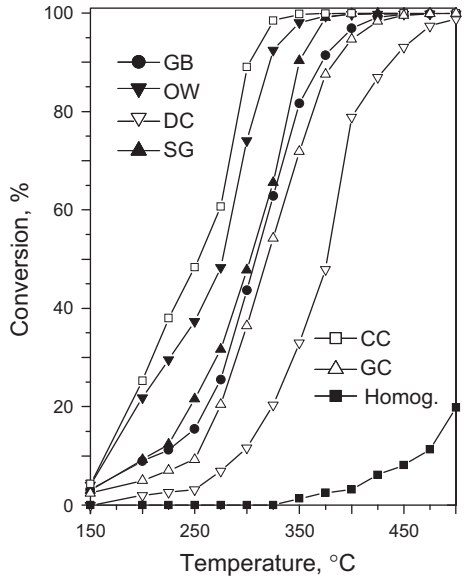

Fig. 4. Light-off curves of DCE oxidation over Co_3O_4 samples activated at 500 °C in air.

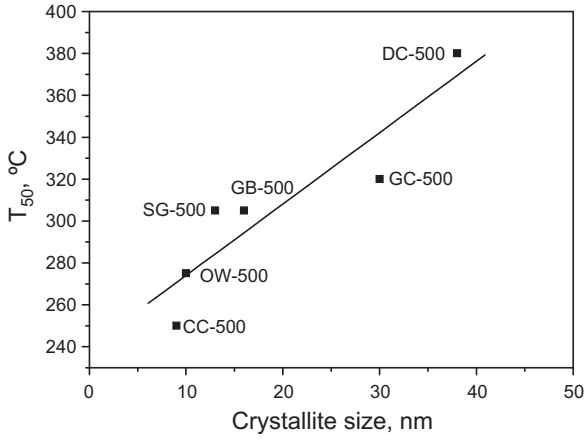

Fig. 5. Relationship between the crystallite size and T_{50} value for the Co_3O_4 samples activated at 500 °C in air.

Although all the cobalt oxide catalysts were comprised of the same phase, Co_3O_4, Fig. 5 suggests that a certain dependence of activity on crystallite size exists, which in turn is very closely related to the redox properties of the samples. As a general behaviour, a lower crystallite size decreased the temperature for DCE 50% conversion. On the basis of the assumption that the reaction occurs through a Mars–Van Krevelen mechanism involving lattice oxygen via a redox cycle [18,21,22], it is believed that the nanocrystalline CC-500 and OW-500 catalysts presented more facile (O^- or O^{2-}) oxygen species that were very reactive for chlorocarbon oxidation. As revealed by H_2-TPR analysis, the reducibility at low temperatures was promoted, and a low-temperature feature on these oxides at 100 °C was also identified, which was not present on other Co_3O_4 samples. The reduced crystallite size of these samples would give rise to a greater number of low coordination defect lattice oxygen sites when compared with more highly crystalline catalysts, and these may significantly contribute to the high activity level [11]. The presence of this type of sites is usually related to the presence of Co^{2+} in the structure of the spinel. For comparative purposes amongst the various synthesised Co_3O_4 samples, the relative abundance of Co^{2+} can be estimated by Raman spectroscopy, since a shift of the A_{1g} vibration towards lower frequencies can be taken as a sensitive indication of a highly defective structure [12]. Typically, five Raman bands at 198, 484, 522, 622 and 694 cm^{-1} are visible in the range 100–800 cm^{-1}, which correspond respectively to the F^1_{2g}, E_g, F^2_{2g}, F^3_{3g} and A_{1g} modes of crystalline Co_3O_4. Results included in Fig. 6 suggest that both highly active CC-500 and OW-500 samples (with a more significant shift of the band, from 694 cm^{-1} for DC-500 to 692–679 cm^{-1}) could present a higher concentration of cobalt in low state, which in turn could indicate oxygen defects.

Taking into account that the second step of the redox model of Mars–Van Krevelen consists of the re-oxidation of the reduced metal oxide sites by the oxygen present in the gas phase, it is important to establish the ability of the catalyst to recover its original oxidised phase (Co_3O_4). The oxygen storage complete capacity (OSCC) is proposed as a meaningful analysis, since it represents the total amount of O_2 consumed after reduction at constant temperature. Fig. 7 includes the OSCC values at 500 °C for some selected samples, namely CC-500, OW-500, SG-500 and DC-500. These values were taken after isothermal reduction between 150 and 350 °C. It was found that CC-500 sample had a superior oxidation behaviour followed by OW-500. However, the other two examined oxides a significantly lower O_2 uptake after reduction. In short, analysis from both H_2-TPR and OSCC showed a better redox behaviour for CC-500 and OW-500 oxides, resulting in an excellent catalytic activity.

Results included in Fig. 5 also suggest that, apart from crystallite size, other catalytic properties may play a role in determining

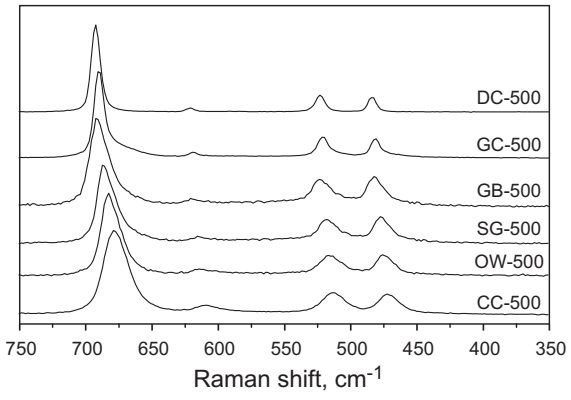

Fig. 6. Raman spectra of the Co_3O_4 samples activated at 500 °C.

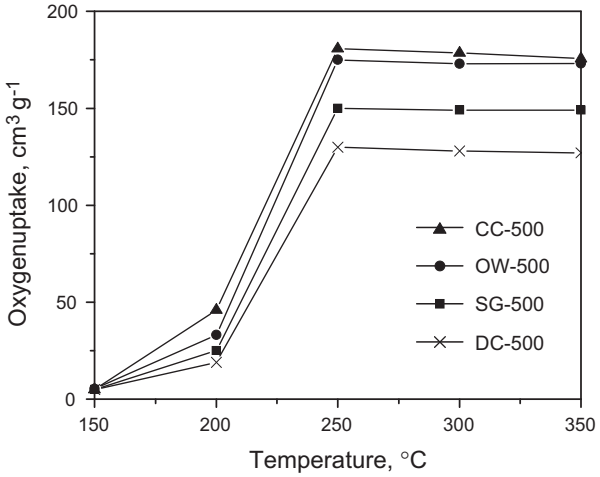

Fig. 7. OSCC of selected Co_3O_4 samples (activated at 500 °C) at varying reduction temperatures.

the overall behaviour of a given bulk cobalt catalyst. This observation stems from the following evidence. On one hand, it was found that both CC-500 and OW-500 samples showed a significantly different activity in spite of having a virtually identical crystallite size (9–10 nm). This behaviour could be related to the notably higher acidity of the CC-500 sample (0.34 mmol NH_3 g^{-1}) in comparison with the OW-500 oxide (0.16 mmol NH_3 g^{-1}). The relevant catalytic role of acidity was also assessed when analysing the activity of SG-500 and GB-500 samples. These two oxides showed a similar T_{50} value, although the crystallite size of SG-500 was appreciably smaller (13 nm versus 16 nm for GB-500). It is believed that the higher overall acidity of GB-500 oxide (0.28 mmol NH_3 g^{-1} in comparison with 0.16 mmol NH_3 g^{-1} for SG-500) was responsible for its notable activity. Acid sites can act as effective chemisorption sites, thus promoting the conversion of the chlorinated feed. Numerous evidence is available to demonstrate the importance of acidity in the overall chlorinated VOC oxidation reaction. For example, both pure Al_2O_3 and ZrO_2 presented a superior activity than non-acidic SiO_2 [23], but proved to be less active when compared with H-zeolites [24,25]. For the latter class of catalysts, it was also found that acid properties could be tuned by selective chemical dealumination for enhancing catalytic performance [26]. Note that the contribution of active oxygen species from the surface of these metal-free samples was negligible. Moreover, when using Ce/Zr or Mn/Zr mixed oxides surface acidity helped in promoting the activity, which was chiefly controlled by the redox properties (accessible lattice oxygen species) at low temperatures [27,28].

3.3. Comparison with other catalysts

Considering the significantly high activity shown by some of the prepared Co_3O_4 catalysts, it is important to compare their behaviour with other previously used examples for chlorinated VOC destruction under identical condition in terms of DCE concentration (1000 ppm in air), total gas flow rate (500 ml min^{-1}) and WHSV $\left(635\ g\ h\ mol^{-1}_{DCE}\right)$, namely alumina supported noble metal catalysts [29], protonic zeolites [24,25], Ce/Zr mixed oxides [27,30,31] and Mn/Zr mixed oxides [28]. These results were obtained within the framework of wider-ranging work conducted in our laboratories on chlorinated VOC oxidation using supported and bulk catalysts (Table 3). It was observed that cobalt oxide samples resulted appreciably more active (T_{50} were lowered by about 15–115 °C with respect to the other catalysts). It is also worth

Table 3
Comparison of DCE oxidation over Co_3O_4 samples with catalysts reported in the literature.

Catalyst	T_{50} (°C)	Reference
H-Y(Si/Al = 2.6)	325	[24]
H-ZSM-5(Si/Al = 27.4)	275	[24]
H-MOR(Si/Al = 5.2)	290	[25]
Dealuminated H-Y(Si/Al = 3.3)	300	[26]
Dealuminated H-Y(Si/Al = 4.3)	280	[26]
Dealuminated H-Y(Si/Al = 6.2)	265	[26]
Dealuminated H-Y(Si/Al = 8.9)	350	[26]
CeO_2	345	[27]
$Ce_{0.8}Zr_{0.2}O_2$	335	[27]
$Ce_{0.68}Zr_{0.32}O_2$	330	[27]
$Ce_{0.5}Zr_{0.5}O_2$	310	[27]
$Ce_{0.15}Zr_{0.85}O_2$	315	[27]
ZrO_2	365	[27]
$Mn_{0.1}Zr_{0.9}O_2$	375	[28]
$Mn_{0.2}Zr_{0.8}O_2$	355	[28]
$Mn_{0.25}Zr_{0.85}O_2$	335	[28]
$Mn_{0.4}Zr_{0.6}O_2$	305	[28]
$Mn_{0.5}Zr_{0.5}O_2$	320	[28]
Mn_2O_3	345	[28]
Al_2O_3	380	[29]
Pt(0.44wt.%)/Al_2O_3	320	[29]
Pd(0.42wt.%)/Al_2O_3	300	[29]
κ-$CeZrO_4$ (pyrochlore)	275	[30]
Co_3O_4 nanoparticles (CC catalyst)	250	This work
Co_3O_4 nanoparticles (OW catalyst)	275	This work

pointing out that although H-zeolites showed considerable activity in DCE abatement with relatively low T_{50} values (265–325 °C), this was somewhat deceptive since the chlorinated feed was mainly converted into chlorinated intermediates, principally vinyl chloride. In fact, 50–70% of the feed was decomposed to this chlorinated species, the complete decomposition of which required temperatures as high as 450 °C. Interestingly, our work shows that selected synthesised Co_3O_4 catalysts can provide a viable alternative to precious metal-based catalysts, the typical reference catalysts for this application.

3.4. Influence of calcination temperature on catalytic performance

In view of the key role played by the Co_3O_4 crystallite size in the combustion of chlorinated hydrocarbons, the behaviour of selected samples calcined at a lower temperature (300 °C for 4 h) was analysed as well. As previously mentioned, this temperature was the minimum temperature required to obtain the desired Co_3O_4 cobalt oxide. In particular, the study was focused on the following active catalysts, namely CC-300, OW-300 and GC-300 oxides. Fig. 8 illustrates the conversion of DCE with reaction temperature for this set of bulk cobalt oxides. These catalysts proved to be highly active, but at 300 °C they only attained 90% conversion. Similar to the conversion trend seen in the series of samples calcined at 500 °C, the CC-300 sample again exhibited the highest activity. On the basis of T_{50} values, the following conversion pattern was found CC-300(200 °C) > OW300(225 °C) > GC-300(250 °C). All these catalysts oxidised DCE at significantly lower temperatures when compared with their counterparts calcined at 500 °C. These samples calcined at 300 °C preserved the same and unique structure (cubic Co_3O_4) but with a substantial higher surface area and smaller crystallite size. Sintering was therefore responsible for this detrimental effect on conversion since it led to an important loss of the amount of accessible catalytic sites. Whilst T_{50} increased from 250 to 320 °C for the GC oxide, a shift of about 50 °C was found for both CC and OW samples. This behaviour was evidence of better thermal stability for these two samples, as the loss of both acid and redox sites was less noticeable compared with that of the GC oxide (Table 1).

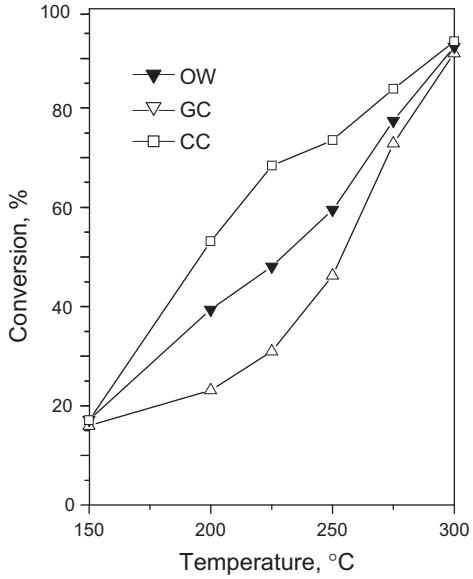

Fig. 8. Light-off curves of DCE oxidation over selected Co_3O_4 samples activated at 300 °C in air.

3.5. Catalyst stability and characterisation of used samples

The catalyst stability of the samples was investigated by analysing the evolution of conversion in a series of consecutive temperature cycles from 150 to 500 °C, and the evolution of conversion with time on stream at 250 °C for 140 h. In the first case, the behaviour of CC-500, OW-500 and SG-500 samples was evaluated. The cycle was repeated four times using the same catalyst. Conversion data for each cycle were super-imposable with no change in the light-off temperature. These observations indicated that the catalyst exhibited stable activity. The used catalysts were characterised by BET measurements, XRD and EDX (Table 4). The BET surface area was seen to decrease by 15–20%, whilst Co_3O_4 crystallite size enlarged significantly, though no evidence of the formation of CoO, with an expected lower catalytic activity, was noted. Moreover, EDX analysis indicated the presence of a significant amount of Cl on the samples between 1.5% and 3.5%. All these changes did not seem to strongly influence the performance of the catalysts. Fig. 9 shows the evolution of conversion over CC-500 catalyst as a function of time on stream (140 h) at 250 °C. This temperature (T_{50}) was selected as it provoked a conversion of less than 100%, thus providing a more sensitive indication of changes of the catalyst performance with time online. These new experiments showed that conversion remained stable (50%) with no appreciable deactivation. By comparing the characterisation results of this sample with those of the sample submitted to four temperature cycles, it was observed that operation over a prolonged time did not lead to a larger decrease in surface area or an increase in crystallite size. Nevertheless, a slightly higher chlorine content was detected (4.2%). An attempt was made to identify the nature of the chlorine present in the sample. Basically, two main possibilities exist in principle, since chlorine may remain adsorbed on the support or interact with the support forming chlorinated species. Results from Raman spectroscopy suggested the formation of $CoCl_2$ characterised by the Raman frequencies at 984 and 1014 cm^{-1}.

3.6. Product distribution

High conversion is not the only criterion for determining good chlorinated VOC destruction catalysts. The desired reaction was

Table 4
Textural, structural and chlorine content of the used Co_3O_4 samples.

Catalyst	BET surface area ($m^2\ g^{-1}$)	Pore volume ($cm^3\ g^{-1}$)	Average pore size (Å)	Crystallite size (nm)	Chlorine content (%)
DC-500[a]	2	0.003	194	52	1.4
GB-500[a]	17	0.05	174	27	2.2
GC-500[a]	15	0.04	325	41	2.9
OW-500[a]	17	0.03	114	17	1.5
CC-500[a]	34	0.19	197	13	3.5
SG-500[a]	16	0.04	158	22	3.1
CC-500[b]	34	0.19	198	13	4.1

[a] After four consecutive temperature cycles from 150 to 500 °C.
[b] After 140 h time on stream at 250 °C.

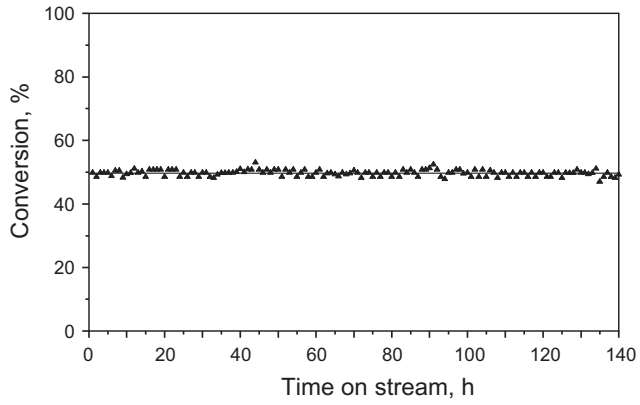

Fig. 9. DCE oxidation over CC-500 sample at 250 °C as a function of time on stream.

Cl-VOC decomposition to deep oxidation products, i.e. CO_2 and HCl or Cl_2. It is indeed useful to provide some basic information about the nature and the amount of reaction products, as the combustion of chlorinated VOCs may be accompanied by the concomitant production of carbon monoxide and highly chlorinated by-products, sometimes more toxic and recalcitrant than the starting material. Next, the product distribution corresponding to the CC-500 sample will be analysed. DCE oxidation gave rise to CO_2, HCl and Cl_2 as major products with a minimal yield of CO. Nevertheless, decomposition was accompanied by the generation vinyl chloride, methyl chloride and carbon tetrachloride at mild temperatures (between 175 and 375 °C) according to Eqs. (3)–(7). Vinyl chloride was formed by dehydrochlorination of the feed molecule, and this by-product could be further partially oxidised to methyl chloride. Carbon tetrachloride was formed as a result of the chlorination of methyl chloride. The peak concentrations were 10–25 ppm (200–225 °C) for vinyl chloride, 250–275 ppm (175 °C) for methyl chloride and 80–100 ppm (350–375 °C) for carbon tetrachloride.

$$C_2H_4Cl_2 \rightarrow C_2H_3Cl + HCl \quad (3)$$
$$C_2H_3Cl + 5/2O_2 \rightarrow 2CO_2 + HCl + H_2O \quad (4)$$
$$C_2H_3Cl + O_2 \rightarrow CH_3Cl + CO_2 \quad (5)$$
$$CH_3Cl + 3/2O_2 \rightarrow CO_2 + HCl + H_2O \quad (6)$$
$$CH_3Cl + 3HCl \rightarrow CCl_4 + 3H_2 \quad (7)$$

With respect to the conversion to carbon oxides, selectivity towards CO_2 was 100% at 400–500 °C. The active performance of Co_3O_4 cobalt oxide for CO oxidation has been previously reported by several authors [6,7]. These results are in stark contrast with those obtained with other bulk catalysts such as protonic zeolites or Ce/Zr mixed oxides. Hence, CO selectivity over the zeolite catalysts was as high as 50–60% [24,26], whilst CO_2 selectivity was about 70–80% over Ce/Zr oxides [27]. On the other hand, conversion of chlorine atoms to HCl was favoured at temperatures lower than 350–400 °C. At higher temperatures, significant amounts of molecular chlorine were also formed due to the occurrence of the Deacon reaction ($2HCl + O_2 \leftrightarrow Cl_2 + H_2O$). As a consequence, selectivity to Cl_2 was about 60–65% at 450–500 °C. It should be pointed out that all of chlorine atoms present in the feed were transformed into HCl or Cl_2, and no other chlorinated by-products were obtained at 350–400 °C.

Product distribution of the oxides activated at 300 °C was also monitored. It was observed that although at 300 °C the chlorinated feed was almost completely decomposed, it was also true that significant amounts of chlorinated by-products were formed. The oxidation of these compounds needed higher temperatures which, in all probability, will modify the structure of the catalyst activated at this low temperature. In contrast, it was seen that for the samples calcined at 500 °C, destruction of the chlorinated by-products occurred below this temperature (500 °C), which points to the existence of an optimum temperature for activation between 300 and 500 °C at which the conversion of the parent molecule to deep oxidation products could be achieved more effectively.

4. Conclusions

The catalytic performance of a series of Co_3O_4 catalysts prepared from a variety of routes was examined for the gas-phase oxidation of 1,2-dichloroethane. This compound was selected as a model chlorinated VOC due to its widespread use in commercial applications and distinct toxicity. A wide number of synthesis routes starting from cobalt(II) nitrate were examined, namely calcination of the precursor salt, solid-state reaction with ammonium hydrogen carbonate or citric acid, precipitation with sodium hydroxide and oxygenated water or sodium carbonate and sol–gel via complexation with citric acid. The resulting oxides were characterised by thermogravimetry, X-ray diffraction, BET measurements, NH_3 temperature-programmed desorption, adsorption of pyridine followed by infrared spectroscopy, Raman spectroscopy, temperature-programmed reduction with hydrogen, oxygen storage complete capacity and energy disperse X-ray analysis.

It was found that although all the routes led to the same phase, substantial differences existed in terms of surface area, crystallite size, and redox and acid properties. In particular, a reduced crystallite size, related in turn to improved redox properties at low temperatures, was seen to be the key factor in determining the activity of the bulk cobalt catalysts. In this sense, of the synthesis procedures investigated, those based on precipitation (via sodium carbonate or sodium hydroxide in the presence of oxygenated water) gave rise to the most active samples with a crystallite size, after thermal stabilisation at 500 °C, about 10 nm. The considerable simplicity of this preparation strategy is noteworthy when taking into account the eventual scale-up of the process. A high total (Lewis) acidity was also observed to be relevant for promoting the conversion of the chlorinated feed. Another important catalytic feature of Co_3O_4 catalysts was that they showed an excellent

100% selectivity towards CO_2. On the other hand, HCl and Cl_2 were the major chlorinated oxidation products with reduced amounts of by-products, which were removed at relatively low temperatures (350–400 °C). Interestingly, these samples (those obtained via precipitation) proved to be considerably more active than supported noble (Pt, Pd) metals, protonic zeolites, and Ce/Zr and Mn/Zr mixed oxides, and were found to be highly stable despite the retention of chlorine on the catalyst surface. This behaviour was evidence of the high potential of this class of catalysts for its widespread application in chlorinated VOC abatement systems. Consequently, it is proposed that future research should be focused on the development of new synthesis routes leading to thermally stable samples with an even lower crystallite size (<10 nm).

Acknowledgment

The authors wish to thank the UPV/EHU-Gobierno Vasco (SAIOTEK S-PE09UN23) for the financial support.

References

[1] J.J. Spivey, in: G. Ertl (Ed.), Handbook of Heterogeneous Catalysis, vol. 5, Wiley-VCH Verlag, Weinheim, 2008, pp. 2394–2411.
[2] A. Szegedi, M. Popova, A. Dimitrova, Z. Cherkezova-Zheleva, I. Mitov, Micropor. Mesopor. Mater. 136 (2010) 106–114.
[3] P. Konova, M. Stoyanova, A. Naydenov, St. Christoskova, D. Mehandjiev, Appl. Catal. 298 (2006) 109–114.
[4] L.F. Liotta, G. Di Carlo, G. Pantaleo, G. Deganello, Appl. Catal. B 70 (2007) 314–322.
[5] Y. Xia, H. Dai, H. Jiang, L. Zhang, Catal. Commun. 11 (2010) 1171–1175.
[6] S. Sun, Q. Gao, H. Wang, J. Zhu, H. Guo, Appl. Catal. B 97 (2010) 284–291.
[7] X. Xie, Y. Li, Z-Q. Liu, M. Haruta, W. Shen, Nature 458 (2009) 746–749.
[8] J. Liu, Z. Zhao, J. Wang, C. Xu, A. Duan, G. Jiang, Q. Yang, Appl. Catal. B 84 (2008) 185–195.
[9] S. Chatterjee, H.L. Greene, Appl. Catal. A 98 (1993) 139–158.
[10] M. Kang, M.W. Song, C.H. Lee, React. Kinet. Catal. Lett. 80 (2003) 123–129.
[11] B. Solsona, I. Vázquez, T. Garcia, T.E. Davies, S.H. Taylor, Catal. Lett. 116 (2007) 116–121.
[12] Q. Liu, L. Wang, M. Chen, Y. Cao, H. He, K. Fan, J. Catal. 263 (2009) 104–113.
[13] C.-B. Wang, C.-C. Lee, J.-L. Bi, J.-Y. Siang, J.-Y. Liu, C.-T. Yeh, Catal. Today 146 (2009) 76–81.
[14] J. Kirchenerova, M. Alifanti, B. Delmon, Appl. Catal. A 231 (2002) 65–80.
[15] R. López-Fonseca, S. Cibrián, J.I. Gutiérrez-Ortiz, M.A. Gutiérrez-Ortiz, J.R. González-Velasco, AIChE J. 49 (2003) 496–504.
[16] X. Wang, X. Chen, L. Gao, H. Zheng, Z. Zhang, Y. Qian, J. Phys. Chem. B 108 (2004) 16401–16404.
[17] H. Yang, Y. Hu, X. Zhang, G. Qiu, J. Phys. Chem. B 107 (2003) 12643–12649.
[18] B. Solsona, T.E. Davies, T. Garcia, I. Vázquez, A. Dejoz, S.H. Taylor, Appl. Catal. B 84 (2008) 176–184.
[19] X. Xie, W. Shen, Nanoscale 1 (2009) 50–60.
[20] R. López-Fonseca, J.I. Gutiérrez-Ortiz, M.A. Gutiérrez-Ortiz, J.R. González-Velasco, J. Chem. Technol. Biotechnol. 78 (2003) 15–22.
[21] G. Busca, M. Daturi, E. Finocchio, V. Lorenzelli, G. Ramis, R.J. Willey, Catal. Today 33 (1997) 239–249.
[22] N. Bahlawane, Appl. Catal. B 67 (2006) 168–176.
[23] J.I. Gutiérrez-Ortiz, R. López-Fonseca, U. Aurrekoetxea, J.R. González-Velasco, J. Catal. 218 (2003) 148–154.
[24] J.R. González-Velasco, R. López-Fonseca, A. Aranzabal, J.I. Gutiérrez-Ortiz, P. Steltenpohl, Appl. Catal. B 24 (2000) 233–242.
[25] R. López-Fonseca, A. Aranzabal, P. Steltenpohl, J.I. Gutiérrez-Ortiz, J.R. González-Velasco, Catal. Today 62 (2000) 367–377.
[26] R. López-Fonseca, B. de Rivas, J.I. Gutiérrez-Ortiz, A. Aranzabal, J.R. González-Velasco, Appl. Catal. B 41 (2003) 31–42.
[27] J.I. Gutiérrez-Ortiz, B. de Rivas, R. López-Fonseca, J.R. González-Velasco, Appl. Catal. A 269 (2004) 147–155.
[28] J.I. Gutiérrez-Ortiz, B. de Rivas, R. López-Fonseca, S. Martín, J.R. González-Velasco, Chemosphere 68 (2007) 1004–1012.
[29] J.R. González-Velasco, A. Aranzabal, J.I. Gutiérrez-Ortiz, R. López-Fonseca, M.A. Gutiérrez-Ortiz, Appl. Catal. B 19 (1998) 189–197.
[30] B. de Rivas, R. López-Fonseca, M.A. Gutiérrez-Ortiz, J.I. Gutiérrez-Ortiz, Appl. Catal. B 101 (2011) 317–325.
[31] B. de Rivas, R. López-Fonseca, C. Sampedro, J.I. Gutiérrez-Ortiz, Appl. Catal. B 90 (2009) 545–555.